Dynamics of Single Hydrogen Bubbles at a Platinum Microelectrode

ARTICLE *in* LANGMUIR · JULY 2015

Impact Factor: 4.46 · DOI: 10.1021/acs.langmuir.5b01825 · Source: PubMed

Langmuir

Article

pubs.acs.org/Langmuir

Dynamics of Single Hydrogen Bubbles at a Platinum Microelectrode

Xuegeng Yang,*[,†] Franziska Karnbach,[‡] Margitta Uhlemann,[‡] Stefan Odenbach,[†] and Kerstin Eckert*[,†]

[†]Institute of Fluid Mechanics, Technische Universität Dresden, D-01069 Dresden, Germany

[‡]IFW Dresden, P.O. Box 270016, D-01171 Dresden, Germany

Supporting Information

ABSTRACT: Bubble dynamics, including the formation, growth, and detachment, of single H_2 bubbles was studied at a platinum microelectrode during the electrolysis of 1 M H_2SO_4 electrolyte. The bubbles were visualized through a microscope by a high-speed camera. Electrochemical measurements were conducted in parallel to measure the transient current. The periodic current oscillations, resulting from the periodic formation and detachment of single bubbles, allow the bubble lifetime and size to be predicted from the transient current. A comparison of the bubble volume calculated from the current and from the recorded bubble image shows a gas evolution efficiency increasing continuously with the growth of the bubble until it reaches 100%. Two different substrates, glass and epoxy, were used to embed the Pt wire. While nearly no difference was found with respect to the growth law for the bubble radius, the contact angle differs strongly for the two types of cell. Data provided for the contact point evolution further complete the image of single hydrogen bubble growth. Finally, the velocity field driven by the detached bubble was measured by means of PIV, and the effects of the convection on the subsequent bubble were evaluated.

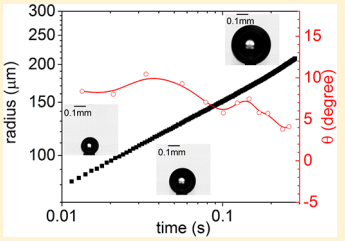

INTRODUCTION

The economic large-scale production of hydrogen is of high interest for both hydrogen-based energy storage systems and mobility systems employing fuel cells. One important piece of technology to produce the required high-purity hydrogen consists of water electrolysis. Commercially, the technique has been used for a long time in alkaline electrolyzers, although its percentage of world production is only around 4%. The possibility to power water electrolysis with renewable energies has increased research in the field of both polymer exchange membranes (PEMs)[1] and alkaline electrolyzers.[2−4] One main challenge in making water electrolysis economically competitive is to raise its efficiency by decreasing the cell voltage. In this respect, electrode coverage by gas bubbles[5−7] is one of the key sources which create undesired overpotentials. Thus, the efficient detachment and transport of gas bubbles away from the electrodes by a corresponding electrode design, zero-gap electrolyzers,[8] or by external fields,[9] as discussed below, is important.

One precondition for efficient bubble management[7] is a detailed understanding of the key mechanisms of hydrogen bubble formation, growth, and detachment. However, despite extensive efforts in the past, important aspects of bubble dynamics, such as the interaction and coalescence of bubbles or the different growth modes of the bubbles themselves, are not yet fully answered. Also, new ways to get rid of large bubbles by means of magnetic fields,[10−14] ultrasound,[15] or supergravity[9] mostly examine the bubble ensemble from the top and not from the side. Hence, to provide that necessary information on the bubble shape profile, including the contact line the bubble forms with the electrode, microelectrodes[16−24] are the method of choice. Here, the multiple growth of several bubbles which shade each other can be largely suppressed and single bubble behavior can be studied in detail. To do so, acid electrolytes, e.g., based on H_2SO_4, are favored in contrast to alkaline ones since highly periodic bubble formation cycles (see, e.g., 18, 21, 24, and 25) can be observed instead of erratic ones. Despite this regularity of bubble formation in acidic electrolytes, the sequence of growth modes, typically expressed by the growth law for the radius R differs significantly between different studies.

$$R(t) = \beta \times t^{b} \tag{1}$$

Agreement exists about a first, inertia-controlled sequence, during which a $R(t) \propto t$ dependence is predicted.[20,26] This was observed in a number of studies,[20,27] although with a poor temporal resolution, restricted mainly to a few data points if at all. The $R(t) \propto t^{1/2}$ regime, as predicted by Scriven[28] for a dynamics controlled by the diffusion of dissolved H_2 toward the bubble, was found to be a succeeding regime by other authors.[16,17,20,27] Other experiments[18] were able to convincingly show that the mass transfer of dissolved hydrogen is not the rate-limiting step and proved that their bubbles follow a $R(t) \propto t^{1/3}$ which was also identified in the other works[19,24,29] in particular for high current densities. Although Westwater and co-workers in their pioneering studies[16,17] found the $t^{1/2}$ dependence for the single bubbles, they also noticed an exponent close to $t^{1/3}$ when coalescing bubbles are present.[16] This fact is interesting because the validity of the growth laws was believed to be restricted to cases where the adhering bubbles do not mutually interfere.[30] Further works, such as refs

Received: May 18, 2015
Revised: June 29, 2015

DOI: 10.1021/acs.langmuir.5b01825
Langmuir XXXX, XXX, XXX−XXX

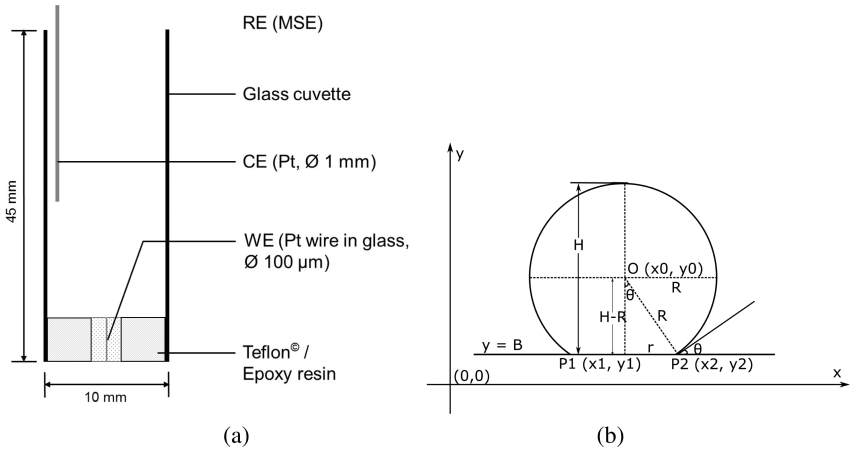

Figure 1. Sketch of (a) electrochemical cell and (b) bubble geometry.

20 and 27 did not only find one or two of these regimes but also reported a continuous transition $t \rightarrow t^{1/2} \rightarrow t^{1/3}$.

A similar diversity is found with respect to the behavior of the contact angle during bubble evolution. The contact angle depends on the wettability of the electrode and on the surface tension of the hydrogen−electrolyte interface. While ref 16 reports on fluctuating contact angles at the Pt electrode in the range of $\theta \sim (5\cdots15)^\circ$ together with a nil overall change, ref 17 reports a permanently decreasing contact angle with increasing bubble radius for the Ni microelectrode and comparable H_2SO_4 concentration, also found in ref 24 for their Pt microelectrode. By contrast, for a larger transparent Pt electrode, ref 24 shows significantly higher contact angles which even slightly increases with growing R.

The present work aims to resolve some of these issues in a combination of high-speed microscopy coupled with extensive image processing and electrochemical measurements. Particular emphasis is also given to a precise description of the bubble geometry, by providing time-resolved data not yet available in the literature. Furthermore, particle image velocimetry is used to study the detachment-induced microconvection of the bubbles and its impact on succeeding bubbles.

EXPERIMENTAL METHODS

Electrochemical Setup. A 3-electrode electrochemical setup was used to generate a single H_2 bubble in 1 M H_2SO_4 electrolyte (Figure 1a). A cuboid glass cuvette (Hellma) with the dimension of height × width × depth = 45 × 10 × 10 mm^3 was used as the electrochemical cell. The working electrode was made from a 100 μm Pt wire with a purity of 99.99%. The cell was manufactured in two different versions. The first type is free of any organic components and was produced by means of burning the Pt wire into a glass capillary. This capillary was inserted into a Teflon plate. For the second type, epoxy resin was used to embed the Pt wire to prepare the working electrode. The Pt surface for both cell versions was polished with SiC paper, ending with #4000. The bottom of the glass cuboid cell was cut to mount the Teflon or epoxy plate with the Pt electrode inside. A Pt wire with a diameter of 1 mm was used as the counter electrode and the mercury/mercurous sulfate electrode (MSE) served as the reference electrode through a salt bridge. All of the potentials refer to the MSE (650 mV vs SHE). The measurements were conducted in a Pt glass cell if not otherwise noted in the article.

Electrolysis was carried out at potentiostatic conditions with a Zahner Zennium electrochemical workstation at −1.5 V for 600 s with a sampling rate of 100 Hz. The glass cell and Teflon plate were cleaned with Caro's acid and rinsed carefully with deionized water before performing the first measurement. Before every further series of experiments, the cell and electrode were cleaned 3 times with distilled water and fresh electrolyte. After the experiments, the glass cell was filled with distilled water so that the Pt electrode was preserved under wet conditions. Before the next series of experiments, the glass cell was treated with the same rinsing procedure as detailed above.

A microscope was used to visualize the gas bubble in side view with a magnification between 10 and 40. The illumination was a LED light together with a diffuser at the back of the cell. The bubble growing videos were taken by a high speed camera (IDT NX4-S1) with a frame rate from 100 to 4000 frames per second (fps) which was increased to 10000 fps in a few experiments. One video containing 1000 to 4600 frames of images was recorded each minute throughout the measurements. The videos were then converted to images for further analysis. To visualize the flow field, tracer particles (polystyrene particles with a size of 1 μm) were added to the electrolyte. These experiments were performed exclusively in the Pt epoxy cell to avoid any contamination by surface-active species in the Pt glass cell.

Description of the Bubble Geometry. The extraction of the bubble geometry, depicted in Figure 1, as a function of time was done via image processing of the high-speed movies and is detailed in the Supporting Information. Three different strategies to assess the key quantity, the bubble radius R, were adopted: (i) R was determined via the Feret diameter, defined as the longest distance between two points in the selected area, using the ImageJ "analyze particle" method; (ii) R was obtained by direct measurement in the gray-value image assuming that the maximum width of the bubble equals the diameter of the bubble; and (iii) fitting of the bubble interface assuming the bubble as a part of a sphere. For this purpose, a circular fit of the bubble interface by Matlab was performed to obtain the equation of a circle for the interface of the hydrogen bubble, given by

$$(x - x_0)^2 + (y - y_0)^2 = R^2 \tag{2}$$

To speed up the number of iterations and the accuracy of the fitting procedure of R and the bubble center (x_0,y_0), initial values of the three quantities were determined by measurement in the gray-value image (see Supporting Information).

From the fit, the height, H, of the bubble can be derived as follows:

$$H = (y_0 - B) + R \tag{3}$$

The volume V of the hydrogen bubble then follows via

$$V = \pi \times H^2 \times (R - H/3) \tag{4}$$

One example to compare the three methods is shown in the Supporting Information. The Feret diameter is bigger than the real value due to the difficulty in distinguishing the bubble by simple threshold analysis. Furthermore, it is clearly seen that the width of the bubble, directly measured in the gray-value image, fits well to the diameter calculated by the circular fit.

DOI: 10.1021/acs.langmuir.5b01825
Langmuir XXXX, XXX, XXX−XXX

Further, important quantities of the bubble are the location of the contact line where the bubble forms on the electrode, and the corresponding contact angle; cf. Figure 1b. Both quantities can be readily derived when the equation for the electrode position is given together with the equation of the circle,

$$y = B \tag{5}$$

To do so, we substitute eq 5 into eq 2 and solve for the zeroes

$$x_{1,2} = x_0 \pm \sqrt{R^2 - (B - y_0)^2} \tag{6}$$

The two solutions x_1 and x_2 are the x coordinates of contact points P_1 and P_2 in Figure 1. The diameter d of the circular contact line which encompasses that area of the electrode covered by the hydrogen bubble is given by

$$d = x_2 - x_1 \tag{7}$$

The contact angle which the liquid−gas interface forms with the Pt electrode can be determined from the slope dy/dx obtained upon differentiating eq 2 with respect to x to obtain $dy/dx = -(x - x_0)/(y - y_0)$. The contact angle, θ, then follows via $\theta = \arctan(x_1 - x_0)/(y_1 - y_0)$. Alternatively, the contact angle can be calculated based on the H and R, obtained as described above:

$$\theta = \arccos \frac{H - R}{R} \tag{8}$$

In the Supporting Information, one example compares the two methods of contact angle determination. The result showed a good agreement of both methods most of the time, but the circular-fit method showed fewer variations from the mean value.

Frequently, another method is used in the literature,[24] termed the "footprint method", in which R and r are the radii of the bubble and of the contact line, respectively.

$$\theta = \arcsin \frac{r}{R} \tag{9}$$

This method needs to measure the footprint of the bubble, which was possible in ref 24 by using a transparent substrate. In the standard case of a nontransparent electrode, in particular when small coalescing bubbles are generated at the rim of the larger bubble, this method is difficult to apply.

On the basis of the issues discussed above, the circular fit method turns out to be the method of choice in the automated processing of large numbers of bubble images. It is therefore used for both radius and contact angle determinations if not indicated otherwise. Before doing this, we checked the accuracy of the method by determining the R and θ of synthetic bubbles, supposed to grow via $R(t) = \beta t^{1/3}$ (see Supporting Information). Here, it turned out that the accuracy of the R determination is better than 0.5 pixels. However, the determination of the contact line diameter is affected with a typical error of ±10 pixels, related to the uncertainty in the determination of the bubble center. Therefore, the uncertainty of the θ determination is ±2°.

RESULTS

The experiments were conducted over a timespan of 600 s during which electrochemical and microscopic measurements ran in parallel. At the given potential, $E = -1500$ mV, applied at the Pt microelectrode, the current−time transient passes periodic current oscillations. A subsequence containing 15 oscillations is depicted in Figure 2a. Parallel microscopic observation shows that each period of the current oscillation is the manifestation of a hydrogen bubble cycle, starting with the formation of the bubble and terminating by its detachment from the electrode. In Figure 2b, we compare the lifetime τ of the gas bubble, determined via microscopy, to the period, τ_{EC}, of the current−time plot, calculated by Matlab. The lifetime provided by both techniques differs by not more than 20 ms (3%) at maximum. Figure 2b shows that the lifetime increases

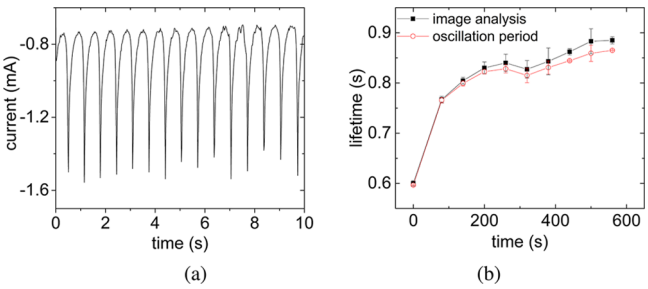

Figure 2. (a) Ten second section taken from the current−time behavior over 600 s at $E = -1.5$ V. (b) The change of period τ_{EC} of the current oscillations obtained from panel a in comparison to the bubble lifetime τ determined by microscopy as a function of time. All experiments were performed in a Pt-glass cell.

with progressing time. The origin is seen in a change of the electrode conditions due the adsorption of H atoms and other species at the Pt surface at longer operation times.

Before going into the dynamics of the bubble cycles, it is worth commenting on the waiting time, Δt_w, until the first hydrogen bubble is formed. Δt_w was discussed by Glas and Westwater[17] for different electrode materials. For hydrogen bubbles evolving at the Ni electrode, a Δt_w up to 30 s was observed for $j = 400$ A/m^2. Actually, there was no measurable waiting time in our experiments. Indeed, microscopic inspection with a high frame rate (10000 fps) shows that the first bubbles form in $\Delta t_w < 0.1$ ms after the potential was applied at the Pt microelectrode exposed to a fresh electrolyte. This signals the existence of a sufficiently large number of nucleation sites at the electrode.

With a given hydrogen diffusivity D ($D = 4.2 \times 10^{-9}$ m^2/s)[31] in the electrolyte, the front of dissolved hydrogen travels over a distance $\delta \sim (D \times \Delta t)^{1/2}$. To estimate the resulting average concentration of dissolved hydrogen c_{H_2}, we consider a small hemispherical volume V_c of a radial extension $R_0 + \delta$ and a height δ above the electrode. Applying eq 4 under the constraint of $R_0 \gg \delta$, we obtain $V_c = 2\pi R_0^2 \times \delta$. The concentration $c_{H_2} = \dot{n}_{H_2} \Delta t_w / V_c$ is then given by

$$c_{H_2} = 2I\sqrt{\Delta t_w} / (zF\pi R_0^2 \sqrt{D}) \tag{10}$$

using Faraday's law. $\dot{n}_{H_2}$ is the number of moles of dissolved hydrogen generated per time; I, F and z refer to the current, the Faraday constant, $F = 96500$ C/mol and the number of electrons involved ($z = 2$). c_{H_2} scales with $(\Delta t_w)^{1/2}$. Setting $I \sim 1.5$ mA and $\Delta t_w \sim 10^{-4}$ s, in accordance with our experimental conditions, we obtain $c_{H_2} = 0.3$ mol/L.

Taking into account the saturation concentration $c^s_{H_2}$ of H_2 of approximately 0.75×10^{-3} mol/L (28 °C),[17] the supersaturation is $\Delta c_{H_2} = c_{H_2} - c^s_{H_2} \sim 0.29$ mol/L. This value slightly exceeds the values in the literature.[17,31,32] Vogt[31] was able to show that the rather different values of Δc_{H_2} in 1 M H_2SO_4 reported by refs 32 (0.1 mol/L for $j = 10^4$A/m^2) and 17 (0.05 mol/L, same current) belong to different regions, the electrode and bulk, respectively. Hence, in view of the rather high current density, the estimated supersaturation close to the electrode is sufficient to achieve bubble nucleation even for very short Δt_w.

H_2 Bubble Cycle. To analyze the bubble cycle in more detail, Figure 3 shows a zoomed in view of one period of the current oscillations together with representative stages (A−F)

DOI: 10.1021/acs.langmuir.5b01825
Langmuir XXXX, XXX, XXX−XXX

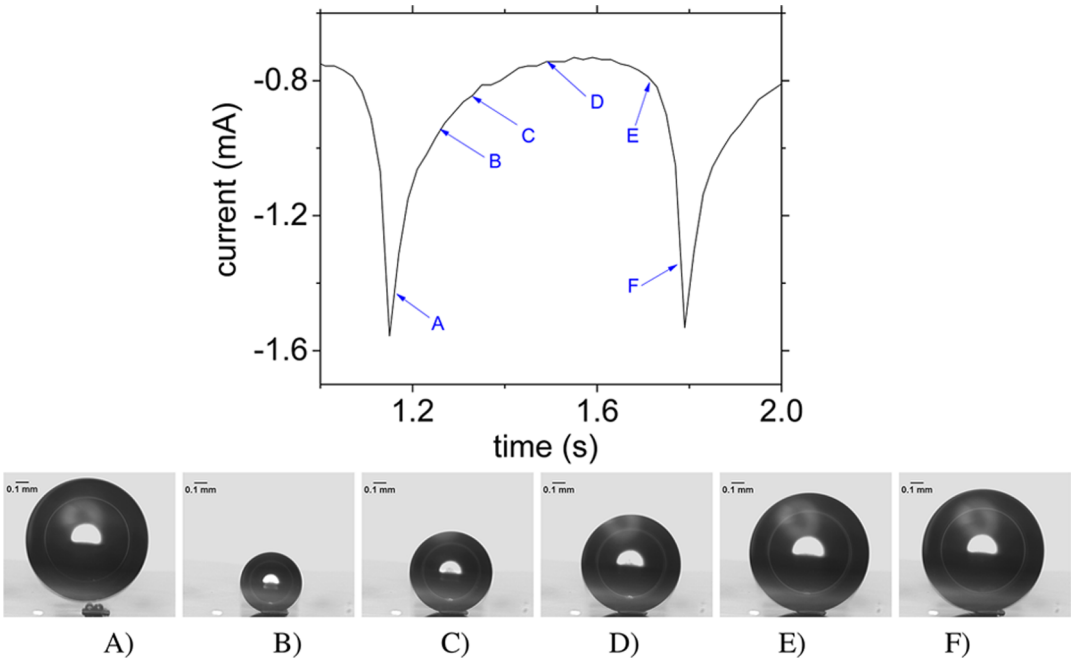

Figure 3. Zoom into a period of the current−time behavior at $E = -1.5$ V with peaks in the current (−1.55 mA) occurring at $t_0 = (1.15 \pm 0.01)$ s and $t = t_0 + \tau$. Characteristic stages of the bubble evolution, denoted by A−F (from left to right), are shown below. Frame A was taken at $t = t_0 + 0.01$ s. All experiments were performed in a Pt-glass cell.

of the corresponding bubbles gained from microscopy. The synchronization between the application of the electric potential and the video signal reveals the coincidence of the moment of bubble detachment and the minimum of I. Thus, every bubble cycle starts with a high current when the large precursor bubble has just detached from the electrode, and the latter is only covered by the first few small hydrogen bubbles. Point A shows an image close to this moment. As the growing bubble increases in size (points B−C), the total current decreases, reaching a minimum at about 60% of τ ($0.6 \times \tau$) around point D. Before the bubble detaches (point F), the current increases again (point E). This interesting but surprising behavior is very robust. It is correlated by a small translation of the bubble along the electrode. This leads to a reduction of the covered electrode area, as will be shown later on. The process of detachment is always accompanied by the immediate formation of small bubbles. They rapidly coalesce to form the next larger bubble, the growth of which then dominates the bubble cycle.

Growth mode of the bubbles. Following Darby and Haque,[18] the temporal change, $\dot{n}_{H_2}$, of the moles of dissolved hydrogen in the electrolyte (volume V_l) between the electrode and bubble is given by the difference between the production of hydrogen per second at the electrode, $\dot{n}_I$, and the consumption, $\dot{n}_b$, by the growing bubble (volume V):

$$\dot{n}_{H_2} = \dot{n}_I - \dot{n}_b \tag{11}$$

$$\frac{1}{V_l}\partial_t C_{H_2} = \frac{I}{zF} - \frac{p}{R_g T}\partial_t V \tag{12}$$

The ideal gas equation $pV = n_b R_g T$ was invoked in the second term of eq 12 to relate n_b to the volume of hydrogen produced under a pressure p and a temperature T at a given gas constant R_g. For the pressure, $p = p_0 + \rho gh + 2\sigma/R$ holds, where p_0, ρgh, and $2\sigma/R$ refer to the atmospheric pressure ($p_0 = 101325$ Pa), the hydrostatic, and the Laplace pressure, respectively. Note that even for the smallest bubble size, $R = 20$ μm, observed in the experiments, the relationship $2\sigma/R = 0.04\ p_0$ holds. Hence, the Laplace pressure can safely be neglected during most of the bubble evolution. The same holds for the hydrostatic pressure in view of the small electrolyte height ($h = 0.03$ m), i.e., $\rho gh = 0.003 p_0$.

On the basis of the fact that the bubble diameter soon becomes larger than that of the electrode, we assume that the change in the hydrogen concentration around the bubble is nil, i.e. $1/V_l \partial_t C_{H_2} = 0$. Thus, we test the validity of the assumption that the hydrogen produced at the electrode directly diffuses into the bubble. This diffusion can only proceed via the thin electrolyte wedge at the foot of the bubble. This wedge starts at the triple point where the three phases (Pt, H_2, and electrolyte) are simultaneously present. The bubble growth law under this condition is then given by

$$\frac{\partial V}{\partial t} = \frac{4\pi}{3}\frac{d(R^3)}{dt} = \frac{I R_g T}{2F p_0} \tag{13}$$

Integration of eq 13 over time delivers

$$V_{EC} = \frac{R_g T}{2F p_0}\int_0^t I dt \tag{14}$$

where the integral $Q = -\int I dt$ was computed with a time resolution of $dt = 0.01$ s. The resulting V_{EC} refers to the volume obtained by measuring the current transient under the assumption of a 100% conversion of the electric current into hydrogen. V_{EC} is plotted as a black curve in Figure 4. Assuming, for the sake of simplicity, a roughly constant current $\bar{I}$ during bubble growth, integrating eq 13 delivers in terms of the bubble radius, i.e., the growth law for high current densities as already introduced in the Introduction.

DOI: 10.1021/acs.langmuir.5b01825
Langmuir XXXX, XXX, XXX−XXX

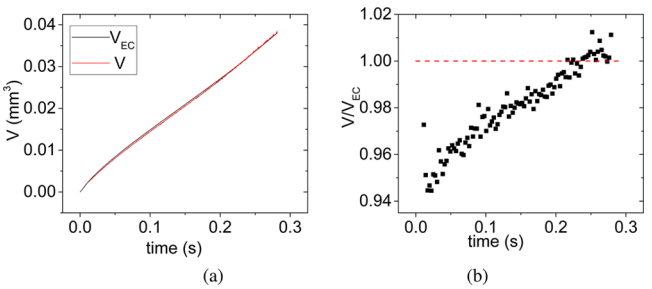

Figure 4. (a) Comparison between the bubble volumes determined by image analysis, V, and calculation, V_{EC}, according to eq 14. t = 0 s corresponds in panel a to the time when the current reaches the peak current and in panel b to the time when the new bubble forms after the previous one has just detached. (b) Ratio V/V_{EC} between the image analysis and calculated bubble volumes; the red dashed line corresponds to V/V_{EC} = 1. The measurement was done in a glass cell with a frame rate of 4000 fps.

$$R = \left(\frac{3\bar{I}R_gT}{8\pi F p_0}\right)^{1/3} t^{1/3} = \beta t^{1/3} \tag{15}$$

V_{EC} is faced with volume V, as obtained by microscopy and applying eq 4, which is plotted as a red curve in Figure 4a. Obviously, the two volumes correspond very well most of the time. To underline the differences, in Figure 4b, we plot the ratio V/V_{EC}, frequently denoted as the gas evolution efficiency. Even at the beginning, the gas efficiency is higher than 0.94 and increases continuously. It reaches unity after approximately 80% of the bubble period. Hence, it is reasonable to assume that nearly 100% of the hydrogen is converted into gas injected into the bubble at its foot. Thus, hydrogen diffusion from the bulk, which would lead to $R \propto t^{1/2}$, does not take place.

A special feature of all experiments in both the Pt glass and the Pt epoxy cell is the fact that the bubble growth also proceeds via coalescence with small hydrogen bubbles. They form in the vicinity of the contact line of the large bubble as documented in Figure 5. This observation differs from the experiments of Kristof and Pritzker[21] who found no coalescence at all in 1 M H_2SO_4. In our case, one could assume that the growth law, eq 13, should be modified into $\partial_t V_b \approx qV_s f_{co}$, where q refers to the number of small bubbles with a volume V_s which coalesces with a rate f_{co}. The experiments show that the size of the small bubbles is about 20 μm. Approximately, three small bubbles ($q \sim 3$) seem to coalesce within 1 ms. However, to create the volume increment of Figure 4, approximately 15 bubbles of this size are necessary. Hence, it is unlikely that the bubble will be totally pumped up via coalescence with small bubbles, but we are faced up to the interesting situation in which the bubble is fed by two different mechanisms at a comparable extent, coalescence and diffusion of hydrogen via the electrolyte wedge. In the next section, we will also see whether this has an impact on the growth law, eq 1.

Evolution of Bubble Geometry. To analyze the growth of the single hydrogen bubbles, we next examine the bubble radius R, the contact angle θ, and the radius of the contact line $r = d/2$ as a function of time. Figure 6a shows R and θ, captured with a frame rate of 4000 fps, versus time in double logarithmic form for the Pt epoxy-cell. The Pt glass and Pt epoxy differ mainly in the evolution of the contact angle (Figure 6b), while the radius evolution proceeds very similarly. Two ranges of radius evolution $R(t)$, eq 1, can be identified, characterized by different slopes as indicated in Figure 6a. The first range captures the early and the intermediate phases of the growing bubble. In contrast to other works,[20,27] we could not identify the linear scaling $R(t) \propto t$ in the early phase as predicted by Rayleigh's equation, $R(t) = (2\Delta p/3\rho_l)^{1/2} \times t$, where Δp and ρ_l refer to the capillary pressure and density of the electrolyte, respectively. Although the initial phase until approximately $t \sim$

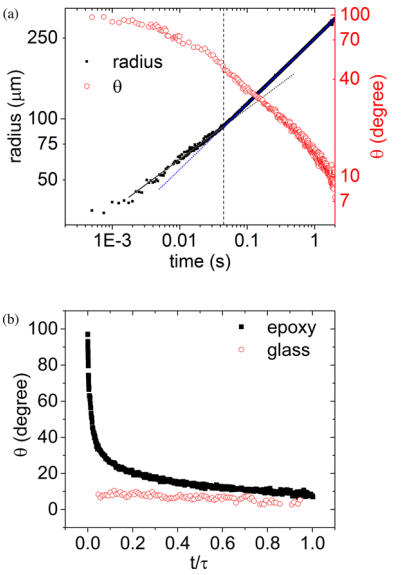

Figure 6. (a) Radius and contact angle versus time during the entire experiment time (epoxy cell; frame rate, 4000 fps). The solid lines in the plot show the linear fit of the radius. The fits are prolonged (dotted lines) to clearly indicate the two different slopes separated by the dashed vertical line. (b) Comparison of the contact angle evolution of the H_2 bubble between the glass (frame rate: 4000 fps) and the epoxy cell.

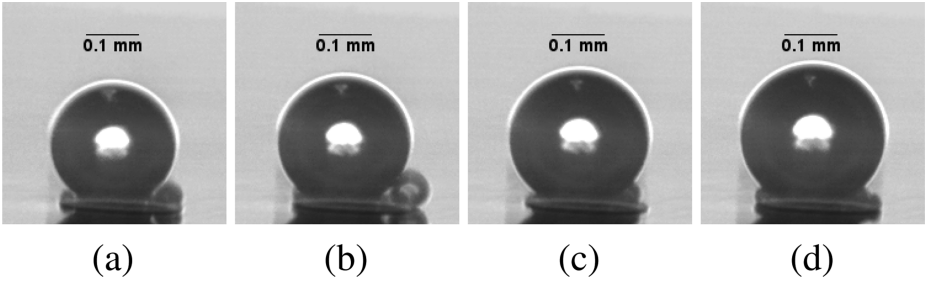

Figure 5. Coalescence of small bubbles with the main bubble; frame rate, 1000 fps. (a) t_0, (b) $t = t_0 + 1$ ms, (c) $t = t_0 + 2$ ms, and (d) $t = t_0 + 3$ ms. All experiments were performed in a Pt-glass cell.

DOI: 10.1021/acs.langmuir.5b01825
Langmuir XXXX, XXX, XXX−XXX

3 ms can be linearly fitted according to $R = a \times t$, the slope a does not match the coefficient of the Rayleigh equation. This behavior is plausible since after 0.1 ms, numerous small bubbles are already present. They coalesce in some milliseconds to form a bigger bubble with a radius of about 40 μm, which is far too large to still obey Rayleigh's equation. During the first regime, the scaling exponent changes smoothly to reach $b = 0.24 \pm 0.02$ at the end.

The second regime is marked by an increase in the slope toward $b = 0.30 \pm 0.02$. This is close to the $R(t) \propto t^{1/3}$ law, discussed above, which follows for the direct diffusion of the hydrogen produced into the bubble via the thin electrolyte wedge at the bottom. An exponent close to 1/3 was already found in the previous works.[18,19,24,27] However, our experiments differ in two aspects from former works. First, as already mentioned before, the growth of the bubble proceeds by two modes, coalescence with small bubbles and diffusion of dissolved H_2. Since the ratio between the volume of the large bubble to that of the small one is much larger than unity, the impact of coalescence on the large bubble remains weak. Under these circumstances, it obviously does not matter from which source hydrogen enters the bubble. Hence, the joint action of both mechanisms leads to a scaling exponent close to 1/3 at high current densities.

Second, different to from refs 16, 17, 20, and 27, a diffusion-controlled regime characterized by a scaling exponent of 1/2 was not observed. We believe that the lack of the diffusion-controlled regime is a natural consequence of the nearly vanishing waiting time until a bubble is formed, both in the fresh electrolyte and after detachment of the forerunning bubble. Hence, in view of the rapid nucleation of hydrogen bubbles, there will be no significant diffusion of dissolved hydrogen into the bulk electrolyte. Thus, it is unlikely to have a regime where the diffusion of dissolved hydrogen from the bulk limits the growth of the bubble.

While $R(t)$ is governed by j (eq 15), the contact angle θ (Figure 6b) is largely determined by the substrate in which the Pt wire is embedded. The hydrophobic epoxy substrate has a surface energy of about 0.046 N/m[33] while that of the hydrophilic glass is about 10 times larger. Hence, the wetting of the hydrophobic epoxy substrate by the acidic electrolyte with its high surface tension (0.073 N/m[34]) is energetically not favorable. Therefore, the contact angle in the epoxy cell is significantly higher than that in the glass cell. As the bubble grows in size, θ showed a power law decrease in the Pt epoxy cell toward the contact angle of the bubble in the glass cell close to detachment. The decreasing θ with increasing R in the epoxy cell, in comparable manner seemingly also found on hydrophobic electrodes,[35] seems to be a logical consequence of the scaling of $R(t) = \beta t^b$ under the condition that r/R is small. In this case, $\theta = \arcsin(r/\beta t^b) \approx (r/\beta)t^{-b}$. Given the growth law, $R(t) = \beta t^{0.28}$ for the particular experiment in the Pt-epoxy cell, on fitting the measured $\theta(t)$, we recover $\theta \approx (r/\beta)t^{-0.28}$. By contrast, in the Pt glass cell θ is with $(10 \pm 2)^\circ$ significantly smaller and decreases much less toward $\theta = (4 \pm 2)^\circ$ close to detachment. In this way, our experiments in the Pt glass cell are in agreement with ref 16 where nearly constant $\theta \sim (5\cdots15)^\circ$ was found with a comparable Pt microelectrode. By contrast, a behavior comparable to our experiments in the Pt epoxy cell was found for similar H_2SO_4 concentration in ref 17 for a Ni microelectrode and[24] for a Pt microelectrode. Meanwhile, with larger planar Pt electrodes, higher and even slightly increasing contact angles were measured.[24]

Returning to the Pt glass cell, the circular fit gives access to the contact points P1 and P2, by means of eqs 6−7 (cf. Figure 1). These points are part of the contact line given by the intersection between the liquid−gas interface and the electrode. Figure 7a (bottom) shows the change in their x-position over time together with the resulting diameter of the contact area, d. Additionally, the x- and y-positions of the bubble center, x_0 and y_0, are plotted in Figure 7a (top). As already mentioned above, the error in determining the diameter of the contact circle, d, is 10 pixels (11 μm) due to an uncertainty in the x-position of P1 and P2 of ±5 pixels. Interestingly, the shape of the d curve shows a fingerprint of the $I-t$ curve (Figure 3a). d rises until the middle of the period to reach an intermediate plateau value which corresponds approximately to the electrode diameter of 100 μm. At times larger than $t/\tau = 0.7$, it decays again to reach approximately 75 μm at detachment. This period of decreasing d is accompanied by a small drift of the x_0 value of the bubble center by about 10 pixels (11 μm) toward smaller x-values along the electrode, which is clearly visible in the videos even to the naked eye. At the same time, a small lift of the bubble occurs; note the stronger increase of y_0 compared to that of the radius R.

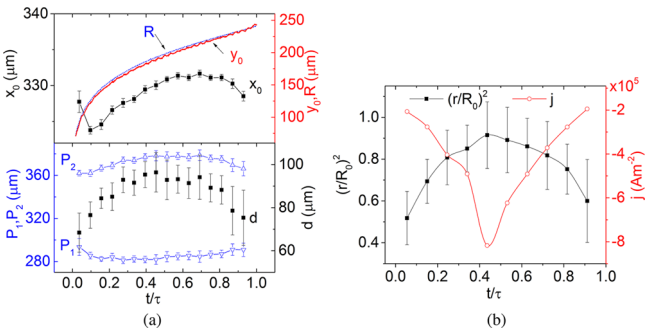

Figure 7. (a) x-Position of contact points, P_1 and P_2, and the resulting contact line diameter (bottom). The top figure shows the center of the bubbles, x_0 and y_0, together with the bubble radius R as a function of time. (b) Ratio between the electrode area covered by the bubble to the entire electrode area superimposed with the current density j. All experiments were performed in a Pt-glass cell at 1000 fps.

In Figure 7b we translate this information into the surface coverage of the electrode by the gas bubble, given by the ratio between contact to electrode area. Notably, this ratio starts to decrease again at about 0.7τ in every bubble cycle. We have superimposed the current density obtained by $j = I/(1-(r/R_0)^2)A_0$ where $A_0 = \pi R_0^2$. We see a significant rise in the current density from 2×10^5 A/m^2 to 8×10^5 A/m^2, i.e., achieved at maximum coverage of the electrode by the bubble.

Detachment Diameter and Lifetime of the Bubbles. Next, the growth dynamics of the bubbles was studied dependent on the saturation of the electrolyte with dissolved hydrogen. Successive measurements were carried out without changing the electrolyte after 600 s of H_2 electrolysis. Figure 8a−b shows the lifetime and detachment radius for the three successive measurements over 600 s, where the pause between these measurements was 60 s. The bubbles shown in both subfigures are from the 10 videos, taken during the 600 s duration, where each video contained approximately 15 bubbles. The lifetime of the bubble increases by about 15% over the duration of the experiment, while the detachment

DOI: 10.1021/acs.langmuir.5b01825
Langmuir XXXX, XXX, XXX−XXX

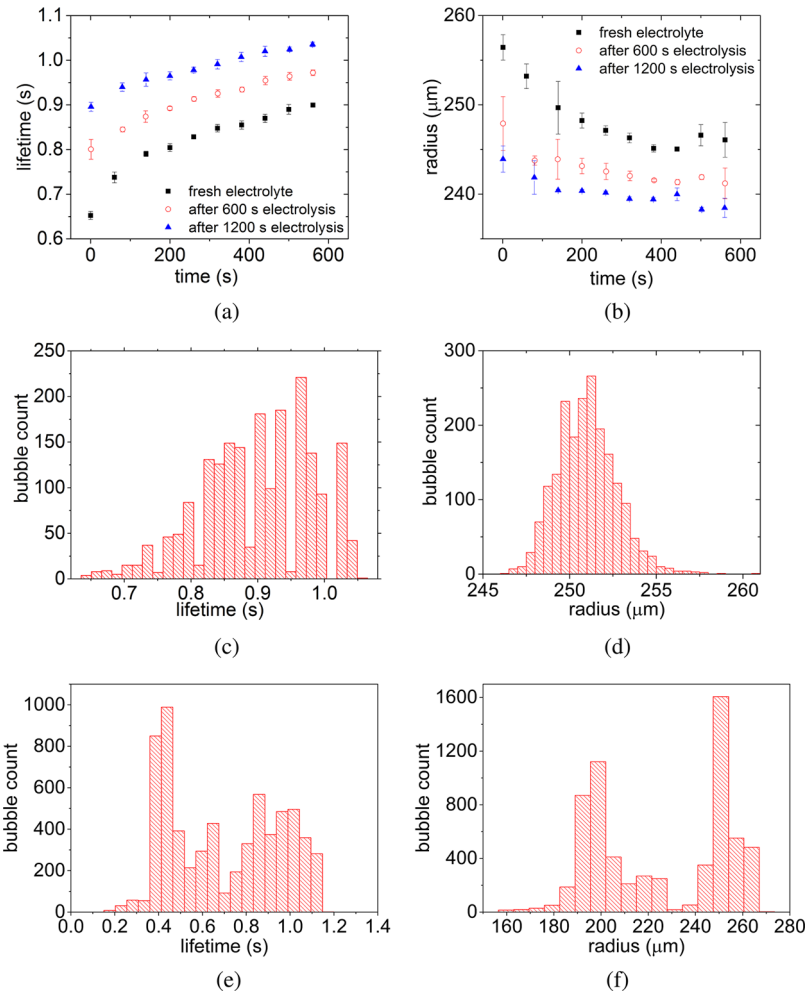

Figure 8. (a–b) Lifetime and the detachment radius of the bubble as a function of time for three subsequent experiments, as indicated in the figure legend. (c–d) Corresponding histograms including all three subsequential measurements in a and b. (e–f) Histograms of lifetime and the detachment radius of the bubble on two different days. All experiments were performed in a Pt-glass cell.

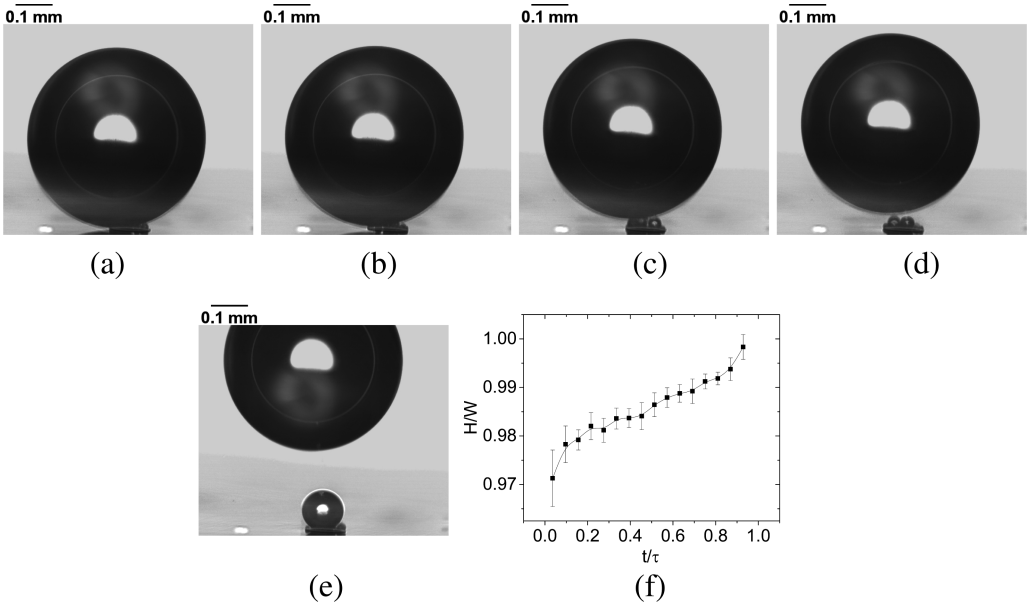

Figure 9. (a–e) Detachment process of the bubble from the electrode in a Pt-epoxy cell; frame rate, 1000fps. The time step between consecutive images is 1 ms. (f) Height-to-width ratio of the bubble versus time.

DOI: 10.1021/acs.langmuir.5b01825
Langmuir XXXX, XXX, XXX–XXX

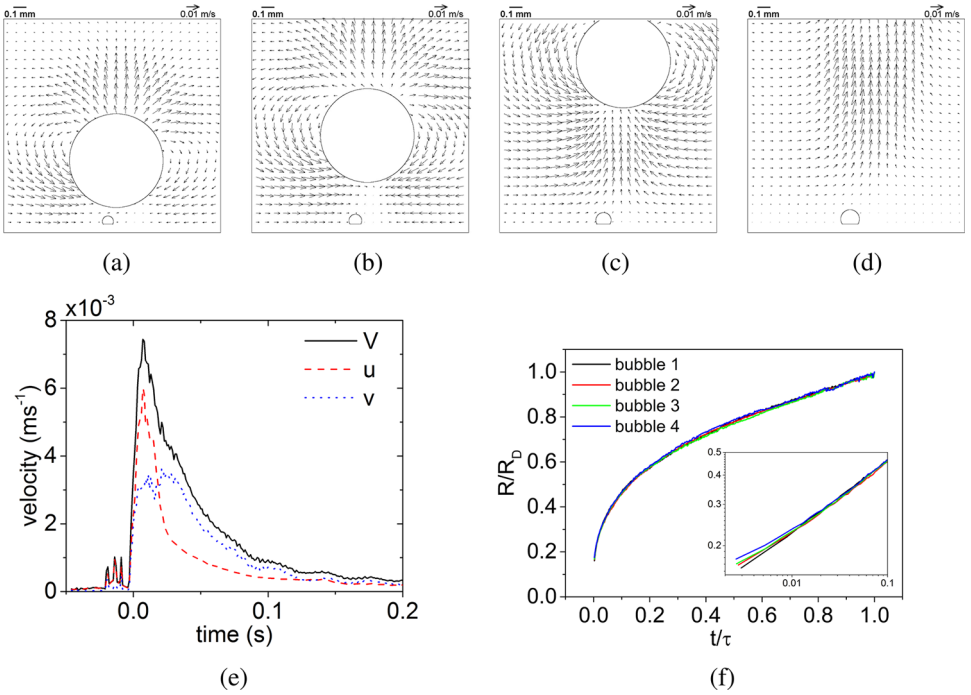

Figure 10. (a–d) Characteristic stages of the flow field during the detachment of a hydrogen bubble. The position and size of the bubble were redrawn in the figures with reference to the real bubble images. (e) Averaged velocity as a function of time. The time when the bubble was detached was set to be zero. (f) Normalized bubble size as a function of time for 4 different bubbles generated at different times after the potential was applied. Bubble 1 was the first when the potential was applied, and bubbles 2, 3, and 4 were the immediately following bubbles. The inset shows a zoomed view of the very early stage of bubble generation where a logarithmic scale was used for a better resolution. The measurement was carried out in an epoxy cell with a frame rate of 1000 fps.

radius decays with time until a steady value is reached. There is only a scatter of 4% in the detachment radii of the three experiments.

The histograms of these 3 experiments are summarized in Figure 8c–d. In contrast to a–b, these data were extracted from the current–time transient and include all bubbles, ca. 600–750 as discussed before. Figure 8d shows a narrow radius distribution with a standard deviation of 1.7 μm. The histogram of the lifetimes does not obey a Gaussian distribution. We assume that the surface of the Pt electrode changes with time by adsorption and absorption of atomic hydrogen during the discharging process. As a result, a slight increase in the overpotential may occur. Because of the charge-controlled mechanism, the absolute value of the current decreases on average, which leads to a slower growth rate, i.e., longer lifetime. This finding is supported by the fact that the bubble growth coefficient β in eq 15 becomes smaller.

Measurements between different days lead to a modified distribution of the lifetime and radius (see Figure 8e–f) even when the electrode/cell assembly is treated as described in the Experimental Methods section. We note a shift of up to 20% in the detachment radius and of about 50% in the lifetime of the bubbles. However, the bubble dynamics is identical to that described before; only the absolute values are shifted. To reduce this scatter, most previous works[17,18,21] were carried out under galvanostatic instead of potentiostatic conditions, as in ref 16 and in the present work. However, the potentiostatic mode of measuring single bubble nucleation, growth and detachment is the manner of choice because it delivers information on how surface conditions change at the Pt electrode. As already pointed out in ref 36, the bubble dynamics at a given potential depends on the polishing quality of the electrode surface and on the history of the electrode with respect to hydrogen penetration into the electrode or aging effects which modify the properties of the surface. Evidence was also found at Pt nanoelectrodes that hydrogen atoms diffuse along the Pt surface toward the Pt glass interface,[37] thereby increasing the effective surface area. Hence, one can safely say that the chemical potential at the Pt surface is changed with time by adsorbed H atoms[38] and other species such as OH^- and H_2O. This is presumed to be the origin of a changed open-circuit potential. The resulting different overpotentials are the source for the shift in Figure 8e–f.

Bubble Detachment and Associated Flow. It is worth looking into the immediate process of the bubble's detachment from the electrode. Five characteristic stages are depicted in 1 ms intervals in Figure 9. Additionally, we have inserted the bubble's aspect ratio defined as the bubble height H divided by the bubble width W (W = 2R). The bubble shape remains very close to that of a sphere, as indicated by a height-to-diameter-ratio which stays close to unity during the entire bubble cycle. Most of the time, the bubble height is slightly smaller than the diameter. With increasing time, the ratio converges to unity. Only in the very last instant of time does a slight increase above unity occur during detachment. In the present case, the process of the bubble's detachment from the electrode differs clearly from that of a bubble emerging from an orifice and hence from other electrolysis experiments showing elongated bubbles.[30,35,39]

In view of the periodic formation of bubbles, the question arises as to whether the detachment of one bubble has an impact on the growth of the successor bubble. This kind of interaction may arise via the flow field which the bubble generates during detachment and lift off, by viscously dragging

DOI: 10.1021/acs.langmuir.5b01825
Langmuir XXXX, XXX, XXX–XXX

the initially stagnant electrolyte. Figure 10a−d shows several characteristic stages of the flow field during bubble detachment. Upon detachment, the bubble rises through the field of view with a velocity of about (120 ± 20) mm/s as determined by tracking the bubble. During this rise, the bubble displaces the electrolyte at its front side which has to be replaced by the electrolyte at its rear side. As a result the new, small bubble which grows at the electrode is impinged upon by a fluid flow. The advection of dissolved hydrogen by this flow strongly depends on the level of hydrogen saturation in the local environment of the electrode and hence on the time history of the experiment. However, the duration of this detachment-induced flow is limited to a short time interval of about 100 ms, as indicated by Figure 10e. This figure plots the startup and decay of this convection. To do so, the components u and v of the velocity vector $\vec{v} = (u,v)$ in the entire area of a−d are area-averaged every time step (cf. Yang et al.[40]), and the average of both as well as of the magnitude of the velocity vector $V = (u^2 + v^2)^{1/2}$ is plotted versus time in e.

Figure 10f examines the evolution of the radius of subsequent bubbles, normalized to the corresponding final detachment radius, versus time, again normalized with the corresponding period τ, for the first four bubbles. Also, the very first bubble which formed in the fresh electrolyte is included. We note that the growth dynamics differ only in the initial phase. Here, we see that the later bubbles are slightly larger at the beginning. However, at the time scale where the detachment-induced convection vanishes, i.e., at around 0.1 s, the curves do again collapse to form one line. For a bubble lifetime of about 0.8 s, we can conclude that the bubble growth in the present Pt microelectrode configuration is only weakly influenced in the very first phase by the detachment-induced convection, but then with almost no impact from the foregoing bubble.

CONCLUSIONS

This study examined the dynamics of a single H_2 bubble generated by water electrolysis in acidic electrolyte on a Pt microelectrode under potentiostatic conditions. Different image analysis methods to investigate the bubble geometry were introduced and compared, among which the self-developed Matlab code provides a fast and automated way to determine the geometry parameters such as the bubble radius, bubble position, and the contact angle. The growth of the single bubble was investigated and compared on two different substrates, glass and epoxy, used to embed the Pt electrode. Nearly independently of the substrate, the bubble radius follows a $R(t) \propto t^{(0.30\pm0.02)}$ law. Hence, the exponent is close to 1/3, as expected for the direct diffusion of the hydrogen produced into the bubble at its foot.

In contrast to R, the contact angle θ of the bubble depends strongly on the material embedding the Pt electrode. It shows an exponential decrease at the hydrophobic epoxy material, while θ with hydrophilic glass shows a much weaker change and stays at low values between (4···12)°.

During the potentiostatic measurements of water electrolysis, the surface conditions of the Pt electrode obviously change. This is mapped by an increase in the bubble lifetime at decreasing detachment radii during the long-term measurement and by a certain shift in both quantities in measurements on different days following otherwise the same dynamics.

In contrast to bubbles detaching from orifices, the hydrogen bubbles are close to sphericity during their entire evolution. If the bubble detaches, a torus-like vortex is formed as the bubble rises. However, at bubble lifetimes of about 0.5 s, hence hydrogen bubble frequencies of about 2 Hz, the wake of this vortex influences the subsequent bubble only marginally during the very first part of its evolution.

Our results have shown that the coalescence of the smaller bubbles at the foot of the bigger bubble is also an important growth mechanism for the present single hydrogen bubbles. A more detailed investigation, in particular with a much higher temporal and spatial resolution, is necessary to shed more light on this problem.

ASSOCIATED CONTENT

Supporting Information

Image processing procedure to obtain the bubble geometry and a comparison of the different methods. The Supporting Information is available free of charge on the ACS Publications website at DOI: 10.1021/acs.langmuir.5b01825.

AUTHOR INFORMATION

Corresponding Authors

*(X.Y.) E-mail: xuegeng.yang@tu-dresden.de.
*(K.E.) E-mail: kerstin.eckert@tu-dresden.de.

Notes

The authors declare no competing financial interest.

ACKNOWLEDGMENTS

Financial support by DFG (Ec201/4) is gratefully acknowledged. We thank K. Hennig for her support and Dres. G. Mutschke, K. Tschulik, Ch. Cierpka, and D. Baczyzmalski for fruitful discussions.

REFERENCES

(1) Carmo, M.; Fritz, D. L.; Mergel, J.; Stolten, D. A comprehensive review on PEM water electrolysis. *Int. J. Hydrogen Energy* **2013**, *38*, 4901−4934.
(2) Ursua, A.; Gandia, L. M.; Sanchis, P. Hydrogen production from water electrolysis: current status and future trends. *Proc. IEEE* **2012**, *100*, 410−426.
(3) Marini, S.; Salvi, P.; Nelli, P.; Pesenti, R.; Villa, M.; Berrettoni, M.; Zangari, G.; Kiros, Y. Advanced alkaline water electrolysis. *Electrochim. Acta* **2012**, *82*, 384−391.
(4) Milewski, J.; Guandalini, G.; Campanari, S. Modeling an alkaline electrolysis cell through reduced-order and loss-estimate approaches. *J. Power Sources* **2014**, *269*, 203−211.
(5) Vogt, H.; Balzer, R. The bubble coverage of gas-evolving electrodes in stagnant electrolytes. *Electrochim. Acta* **2005**, *50*, 2073−2079.
(6) Zeng, K.; Zhang, D. Recent progress in alkaline water electrolysis for hydrogen production and applications. *Prog. Energy Combust. Sci.* **2010**, *36*, 307−326.
(7) Zhang, D.; Zeng, K. Evaluating the behavior of electrolytic gas bubbles and their effect on the cell voltage in alkaline water electrolysis. *Ind. Eng. Chem. Res.* **2012**, *51*, 13825−13832.
(8) Pletcher, D.; Li, X. Prospects for alkaline zero gap water electrolysers for hydrogen production. *Int. J. Hydrogen Energy* **2011**, *36*, 15089−15104.
(9) Wang, M.; Wang, Z.; Gong, X.; Guo, Z. The intensification technologies to water electrolysis for hydrogen production-A review. *Renewable Sustainable Energy Rev.* **2014**, *29*, 573−588.
(10) Iida, T.; Matsushima, H.; Fukunaka, Y. Water electrolysis under a magnetic field. *J. Electrochem. Soc.* **2007**, *154*, E112−E115.
(11) Lin, M.-Y.; Hourng, L.-W.; Kuo, C.-W. The effect of magnetic force on hydrogen production efficiency in water electrolysis. *Int. J. Hydrogen Energy* **2012**, *37*, 1311−1320.

DOI: 10.1021/acs.langmuir.5b01825
Langmuir XXXX, XXX, XXX−XXX

(12) Koza, J. A.; Mühlenhoff, S.; Uhlemann, M.; Eckert, K.; Gebert, A.; Schultz, L. Desorption of hydrogen from an electrode surface under influence of an external magnetic field-In-situ microscopic observations. *Electrochem. Commun.* **2009**, *11*, 425−429.
(13) Koza, J. A.; Mühlenhoff, S.; Żabńiski, P.; Nikrityuk, P. A.; Eckert, K.; Uhlemann, M.; Gebert, A.; Weier, T.; Schultz, L.; Odenbach, S. Hydrogen evolution under the influence of a magnetic field. *Electrochim. Acta* **2011**, *56*, 2665−2675.
(14) Fernández, D.; Diao, Z.; Dunne, P.; Coey, J. Influence of magnetic field on hydrogen reduction and co-reduction in the Cu/CuSO4 system. *Electrochim. Acta* **2010**, *55*, 8664−8672.
(15) Li, S.-D.; Wang, C.-C.; Chen, C.-Y. Cheng-Chien Wang Water electrolysis in the presence of an ultrasonic field. *Electrochim. Acta* **2009**, *54*, 3877−3883.
(16) Westerheide, D. E.; Westwater, J. Isothermal growth of hydrogen bubbles during electrolysis. *AIChE J.* **1961**, *7*, 357−362.
(17) Glas, J.; Westwater, J. Measurements of the growth of electrolytic bubbles. *Int. J. Heat Mass Transfer* **1964**, *7*, 1427−1443.
(18) Darby, R.; Haque, M. The dynamics of electrolytic hydrogen bubble evolution. *Chem. Eng. Sci.* **1973**, *28*, 1129−1138.
(19) Verhaart, H.; De Jonge, R.; Van Stralen, S. Growth rate of a gas bubble during electrolysis in supersaturated liquid. *Int. J. Heat Mass Transfer* **1980**, *23*, 293−299.
(20) Brandon, N.; Kelsall, G. Growth kinetics of bubbles electrogenerated at microelectrodes. *J. Appl. Electrochem.* **1985**, *15*, 475−484.
(21) Kristof, P.; Pritzker, M. Effect of electrolyte composition on the dynamics of hydrogen gas bubble evolution at copper microelectrodes. *J. Appl. Electrochem.* **1997**, *27*, 255−265.
(22) Fernández, D.; Martine, M.; Meagher, A.; Möbius, M. E.; Coey, J. Stabilizing effect of a magnetic field on a gas bubble produced at a microelectrode. *Electrochem. Commun.* **2012**, *18*, 28−32.
(23) Luo, L.; White, H. S. Electrogeneration of Single Nanobubbles at Sub-50-nm-Radius Platinum Nanodisk Electrodes. *Langmuir* **2013**, *29*, 11169−11175.
(24) Fernández, D.; Maurer, P.; Martine, M.; Coey, J.; Möbius, M. E. Bubble formation at a gas-evolving microelectrode. *Langmuir* **2014**, *30*, 13065−13074.
(25) Gabrielli, C.; Huet, F.; Keddam, M.; Sahar, A. Investigation of water electrolysis by spectral analysis. I. Influence of the current density. *J. Appl. Electrochem.* **1989**, *19*, 683−696.
(26) Rayleigh, L., VIII On the pressure developed in a liquid during the collapse of a spherical cavity. *London, Edinburgh, and Dublin Philosophical Magazine and Journal of Science* **1917**, *34*, 94−98.
(27) Sakuma, G.; Fukunaka, Y.; Matsushima, H. Nucleation and growth of electrolytic gas bubbles under microgravity. *Int. J. Hydrogen Energy* **2014**, *39*, 7638−7645.
(28) Scriven, L. On the dynamics of phase growth. *Chem. Eng. Sci.* **1959**, *10*, 1−13.
(29) Dinkelacker, M. Zur Gasentwicklung und Blasenbildung an Elektroden. Ph.D. Thesis, DLR, Institut für Technische Thermodynamik, Stuttgart, Germany,1989.
(30) Vogt, H. *Comprehensive Treatise of Electrochemistry*; Springer: New York, 1983; pp 445−489.
(31) Vogt, H. On the supersaturation of gas in the concentration boundary layer of gas evolving electrodes. *Electrochim. Acta* **1980**, *25*, 527−531.
(32) Shibata, S. *Bull. Chem. Soc. Jpn.* **1963**, *36*, 53.
(33) Comyn, J. *Handbook of Adhesives and Sealants*; Cognard, P., Ed.:, Elsevier: Amsterdam, The Netherlands, 2006; Vol. 2.
(34) Suggitt, R.; Aziz, P.; Wetmore, F. The surface tension of aqueous sulfuric acid solutions at 25°C. *J. Am. Chem. Soc.* **1949**, *71*, 676−678.
(35) Brussieux, C.; Viers, P.; Roustan, H.; Rakib, M. Controlled electrochemical gas bubble release from electrodes entirely and partially covered with hydrophobic materials. *Electrochim. Acta* **2011**, *56*, 7194−7201.
(36) Gabrielli, C.; Huet, F.; Keddam, M. Characterization of electrolytic bubble evolution by spectral analysis. Application to a corroding electrode. *J. Appl. Electrochem.* **1985**, *15*, 503−508.
(37) Zhan, D.; Velmurugan, J.; Mirkin, M. V. Adsorption/desorption of hydrogen on Pt nanoelectrodes: Evidence of surface diffusion and spillover. *J. Am. Chem. Soc.* **2009**, *131*, 14756−14760.
(38) Strmcnik, D.; Tripkovic, D.; van der Vliet, D.; Stamenkovic, V.; Marković, N. Adsorption of hydrogen on Pt (111) and Pt (100) surfaces and its role in the HOR. *Electrochem. Commun.* **2008**, *10*, 1602−1605.
(39) Piontelli, R.; Mazza, B.; Pedeferri, P.; Tognoni, A. Ricerche sullo sviluppo elettrodico di gas e sugli effetti anomali che lo accompagnano, Sviluppo da soluzione acquose. *Electrochim. Metall.* **1967**, *2*, 257−287.
(40) Yang, X.; Eckert, K.; Mühlenhoff, S.; Odenbach, S. On the decay of the Lorentz-force-driven convection in vertical concentration stratification during magnetoelectrolysis. *Electrochim. Acta* **2009**, *54*, 7056−7065.

DOI: 10.1021/acs.langmuir.5b01825
Langmuir XXXX, XXX, XXX−XXX